

Blood-based magnetohydrodynamic Casson hybrid nanofluid flow on convectively heated bi-directional porous stretching sheet with variable porosity and slip constraints

Showkat Ahmad Lone, Rawan Bossly, Fuad S. Alduais, Afrah Al-Bossly, Arshad Khan, Anwar Saeed

Citation: Chin. Phys. B, 2025, 34 (**1**): 014101. DOI: 10.1088/1674-1056/ad8a45
Journal homepage: http://cpb.iphy.ac.cn; http://iopscience.iop.org/cpb

What follows is a list of articles you may be interested in

Theoretical study on the effective thermal conductivity of silica aerogels based on a cross-aligned and cubic pore model

Kuncan Zheng(郑坤灿), Zhendong Li(李震东), Yutong Cao(曹豫通), Ben Liu(刘犇)), and Junlei Hu(胡君磊)
Chin. Phys. B, 2024, 33 (**6**): 064401. DOI: 10.1088/1674-1056/ad47ac

Lattice Boltzmann simulation on thermal performance of composite phase change material based on Voronoi models

Meng-Yue Guo(郭孟月), Qun Han(韩群), Xiang-Dong Liu(刘向东), and Bo Zhou(周博)
Chin. Phys. B, 2021, 30 (**10**): 104401. DOI: 10.1088/1674-1056/ac041d

Shim coil design for Halbach magnet by equivalent magnetic dipole method

Jia-Min Wu(吴嘉敏), Zheng Xu(徐征), Pan Guo(郭盼), Jin-Feng Qi(戚金凤), Yu-Cheng He(贺玉成)
Chin. Phys. B, 2018, 27 (**10**): 104101. DOI: 10.1088/1674-1056/27/10/104101

A double constrained robust capon beamforming based imaging method for early breast cancer detection

Xiao Xia (肖夏), Xu Li (徐立), Li Qin-Wei (李钦伟)
Chin. Phys. B, 2013, 22 (**9**): 094101. DOI: 10.1088/1674-1056/22/9/094101

Enhanced absorption property of ordered mesoporous carbon/Co-doped ordered mesoporous carbon double-layer absorber

Guo Shao-Li (郭绍丽), Wang Liu-Ding (王六定), Wang Yi-Ming (王一明), Wu Hong-Jing (吴宏景), Shen Zhong-Yuan (沈中元)
Chin. Phys. B, 2013, 22 (**4**): 044101. DOI: 10.1088/1674-1056/22/4/044101

Blood-based magnetohydrodynamic Casson hybrid nanofluid flow on convectively heated bi-directional porous stretching sheet with variable porosity and slip constraints

Showkat Ahmad Lone[1], Rawan Bossly[2], Fuad S. Alduais[3], Afrah Al-Bossly[3], Arshad Khan[4,†], and Anwar Saeed[5]

[1] *Department of Basic Sciences, College of Science and Theoretical Studies, Saudi Electronic University, (Jeddah-M), Riyadh*-11673, *Saudi Arabia*
[2] *Department of Mathematics, College of Science, Jazan University, Jazan* 82817, *Saudi Arabia*
[3] *Department of Mathematics, College of Science and Humanities in Al-Kharj, Prince Sattam bin Abdulaziz University, Al-Kharj* 11942, *Saudi Arabia*
[4] *College of Aeronautical Engineering, National University of Sciences and Technology, Sector H*-12, *Islamabad* 44000, *Pakistan*
[5] *Department of Mathematics, Abdul Wali Khan University, Mardan* 23200, *Khyber, Pakhtunkhwa, Pakistan*

(Received 7 July 2024; revised manuscript received 11 September 2024; accepted manuscript online 23 October 2024)

Fluid flow through porous spaces with variable porosity has wide-range applications, notably in biomedical and thermal engineering, where it plays a vital role in comprehending blood flow dynamics within cardiovascular systems, heat transfer and thermal management systems improve efficiency using porous materials with variable porosity. Keeping these important applications in view, in current study blood-based hybrid nanofluid flow has considered on a convectively heated sheet. The sheet exhibits the properties of a porous medium with variable porosity and extends in both the x and y directions. Blood has used as base fluid in which the nanoparticles of Cu and CuO have been mixed. Thermal radiation, space-dependent, and thermal-dependent heat sources have been incorporated into the energy equation, while magnetic effects have been integrated into the momentum equations. Dimensionless variables have employed to transform the modeled equations into dimensionless form and facilitating their solution using bvp4c approach. It has concluded in this study that, both the primary and secondary velocities augmented with upsurge in variable porous factor and declined with escalation in stretching ratio, Casson, magnetic, and slip factors along x- and y-axes. Thermal distribution has grown up with upsurge in Casson factor, magnetic factor, thermal Biot number, and thermal/space-dependent heat sources while has retarded with growth in variable porous and stretching ratio factors. The findings of this investigation have been compared with the existing literature, revealing a strong agreement among present and established results that ensured the validation of the model and method used in this work.

Keywords: hybrid nanofluid, Casson fluid, magnetohydrodynamics, variable porous space, space/thermal-dependent heat sources, velocity slip and thermal convective conditions

PACS: 41.20.Gz, 44.30.+v, 47.35.–i, 52.25.Os, 02.30.Jr

DOI: 10.1088/1674-1056/ad8a45 **CSTR:** 32038.14.CPB.ad8a45

1. Introduction

Nanofluid flow describes to the movement of a fluid containing nanoparticles, typically with dimensions in the nanometer range, dispersed within a base fluid. Nanofluids are engineered colloidal suspensions where nanoparticles are uniformly dispersed in a base fluid, like water and oil, *etc*. These nanoparticles can be metallic, oxide, carbon-based, or other materials, and they exhibit unique thermal, electrical, and mechanical properties compared to the base fluid alone as worked out by Mahian *et al*.[1] Nanofluid flow has gained attention due to its potential applications in various fields, including heat transfer enhancement, cooling systems, biomedical engineering, and energy production.[2,3] Researchers study nanofluid flow to understand its behavior, optimize its thermal properties, and explore its applications in different industries.[4] Bhatti *et al*.[5] inspected Williamson nanofluid flow through permeable circulating pates. Over time, it has been observed that suspensions containing two types of nanoparticles within a pure fluid exhibit improved thermal flow characteristics.[6] Over the years, researchers have observed a significant improvement in thermal flow characteristics within suspensions containing two types of nanoparticles dispersed in a pure fluid. This observation, underscores the growing recognition of the enhanced thermal properties achievable through the strategic combination of nanoparticles in colloidal suspensions.[7,8] This finding suggests promising avenues for advancing heat transfer efficiency in various applications, like thermal management systems, heat exchangers, and cooling technologies.[9] Moreover, this observation highlights the importance of ongoing research efforts in nanofluid dynamics and the potential for further advancements in the field. As nanotechnology continues to evolve, the understanding of complex fluid dynamics in nanoparticle suspensions will undoubtedly contribute to the development of more ef-

†Corresponding author. E-mail: arshad8084@gmail.com

© 2025 Chinese Physical Society and IOP Publishing Ltd. All rights, including for text and data mining, AI training, and similar technologies, are reserved.

ficient and sustainable thermal management solutions across diverse industries. A ternary hybrid nanofluid consists of a base fluid, typically water or oil, combined with three distinct types of nanoparticles, each with unique thermal properties. These nanoparticles, often metallic, oxide, or carbon-based, are dispersed homogeneously within the base fluid to form a stable colloidal suspension.[10] The combination of multiple nanoparticles offers synergistic effects, enhancing the thermal conductivity, heat capacity, and convective heat transfer characteristics of the nanofluid compared to conventional single-component nanofluids.[11] The presence of different types of nanoparticles in pure fluids provides a broader range of applications in heat transfer enhancement.[12] Through careful selection and optimization of nanoparticle types and concentrations, ternary hybrid nanofluids have shown remarkable potential for improving heat transfer efficiency in various engineering applications, including thermal management systems, heat exchangers, and cooling technologies.[13,14] Additionally, the unique thermal properties of ternary hybrid nanofluids offer opportunities for advancements in energy conversion systems, thermal insulation materials, and biomedical applications, contributing to the development of more efficient and sustainable heat transfer solutions across diverse industries.[15]

Casson fluid, a non-Newtonian fluid characterized by a yield stress, exhibits unique rheological properties that significantly impact heat transfer phenomena. Unlike Newtonian fluids, Casson fluids require a minimum stress, known as the yield stress, to initiate flow, making their behavior more complex and nonlinear.[16] This yield stress behavior leads to a nonlinear relationship between shear stress and shear rate, particularly at low shear rates, resulting in a higher apparent viscosity compared to Newtonian fluids. In terms of heat transfer, these rheological characteristics have profound effects on heat transfer phenomenon.[17,18] In forced convection scenarios, such as flow through pipes or over surfaces, the viscosity variation of Casson fluids with shear rate alters the velocity profile and heat transfer coefficient, potentially hindering heat transfer efficiency, especially at low shear rates where viscosity is higher.[19] Moreover, the yield stress behavior influences heat conduction, as Casson fluids can exhibit solid-like behavior at low shear rates or in stagnant regions, limiting heat transfer through conduction compared to more fluid-like behavior.[20] Additionally, in processes involving mixing or stirring, the yield stress can cause non-uniform shear rates, leading to localized variations in temperature distribution within the fluid, further impacting heat transfer rates. These complex rheological properties of Casson fluids is essential for optimizing heat transfer processes in various engineering and scientific applications, guiding the design of more efficient heat exchangers, reactors, and thermal management systems. Khan *et al*.[21] inspected gyrating MHD Casson fluid flow on gyrating cylinder using Joule heating and dissipative effects and have noticed that with growth in Casson factor the fluid flow has declined while thermal transference has augmented. Rasheed *et al*.[22] studied time-dependent Casson fluid flow on a vertical sheet with Hall current and chemical reactivity effects.

Magnetohydrodynamics (MHD) is a multidisciplinary field that studies the behavior of electrically conducting fluids, like plasmas and liquid metals, *etc*. using magnetic fields. In the context of heat transfer, MHD plays a crucial role in various engineering applications, particularly in systems where fluid flow and heat transfer are intimately coupled, like nuclear reactors, MHD generators, and space propulsion systems.[23,24] The interaction between the magnetic field and the fluid induces Lorentz forces, which can significantly alter the flow patterns, heat transfer rates, and overall system performance. In forced convection heat transfer, the Lorentz forces can modify the velocity distribution, leading to changes in boundary layer thickness, flow separation, and turbulence levels, consequently affecting the heat transfer coefficient.[25] Additionally, MHD can influence natural convection processes, where buoyancy-driven flows interact with magnetic fields, resulting in complex flow patterns and enhanced or suppressed heat transfer rates depending on the orientation and strength of the magnetic field.[26] Singh *et al*.[27] discussed MHD convective fluid flow on a vertical sheet and have noticed that flow has vanished for minute quantity of magnetic field. Furthermore, MHD effects can impact thermal management systems, like in liquid metal cooling of advanced nuclear reactors or in the design of MHD pumps for high-temperature applications, where optimizing heat transfer while considering MHD-induced phenomena is essential for system reliability and efficiency.[28] Overall, understanding the interplay between MHD and heat transfer is crucial for advancing technologies in energy production, space exploration, and various industrial processes, driving innovations in thermal engineering and fluid dynamics.

Variable porous space describes a medium where the porosity, or void fraction, varies spatially within the material. This variation in porosity can have significant impacts on heat transfer processes. In regions of higher porosity, fluid flow tends to be more pronounced due to reduced resistance, leading to enhanced convective heat transfer rates.[29] Conversely, regions with lower porosity experience decreased fluid flow and reduced convective heat transfer. This spatial variation in convective heat transfer rates results in non-uniform heat distribution within the porous medium. Additionally, the varying porosity affects the effective thermal conductivity of the

medium, with higher porosity regions exhibiting lower thermal conductivity due to the increased presence of fluid.[30] This spatial variation in thermal conductivity further contributes to non-uniform heat transfer. Furthermore, changes in porosity over time introduce transient effects, altering flow patterns and thermal properties, which in turn influence transient heat transfer behavior within the medium.[31] These impacts are crucial for optimizing the design and performance of systems utilizing variable porous space, such as geothermal energy extraction, underground heat storage, and thermal management of electronic devices, enabling more efficient heat transfer and utilization in various engineering applications.[32] Wahid *et al.*[33] inspected time-dependent three-dimensional (3D) radiative flow of fluid in a permeable contracting sheet with impacts of nanoparticles. From the literature review, it is evident that most studies have focused primarily on surfaces with uniform permeability.

A heat source is a physical entity or mechanism that generates heat energy, typically through processes such as combustion, electrical resistance, nuclear reactions, or chemical reactions. Heat sources play a fundamental role in various engineering and scientific applications, including heating systems, industrial processes, power generation, and thermal management. Fluid flow with a heat source involves the movement of a fluid while heat is being added or removed within a system, impacting heat transfer in various ways.[34,35] The presence of fluid flow enhances convective heat transfer by carrying heat away from the source more efficiently compared to stagnant conditions.[36] Flow patterns induced by the movement of the fluid can also lead to turbulence, which further enhances heat transfer by increasing fluid mixing. However, turbulence can also introduce additional frictional losses and affect system efficiency. Furthermore, the presence of a heat source alters the boundary layer near heated surfaces, influencing convective heat transfer rates.[37] The thickness and characteristics of this boundary layer depend on factors such as flow velocity, fluid properties, and surface roughness, further impacting heat transfer behavior. Sharma *et al.*[38] inspected thermal and exponentially space-dependent heat source for EMHD fluid flow on a stretching vertical surface. Zaydan *et al.*[39] studied fluid flow on a Riga plate with the impacts of space-dependent thermal source. Varun Kumar *et al.*[40] inspected heat transference exploration for fluid flow on a moveable surface with influence of thermal-based exponentially heat source.

From the cited literature it has observed that many investigations have been conducted to discuss thermal transportation using various flow conditions including heat source, thermal radiations, thermal slip conditions, uniform porous space, and MHD effects, *etc*. But no investigation has yet been conducted to examine thermal enhancement with combined effects of space-dependent heat source and thermal-dependent heat source on a variable porous space, which creates a gap in existing literature that highlights an area which has not yet been thoroughly investigated. To fill this gap, in current study blood-based hybrid nanofluid flow has considered on a convectively heated sheet. The sheet exhibits the properties of a variable porous medium and extends in both the x and y directions. Thermal radiation, space-dependent, and thermal-dependent heat sources have been incorporated into the energy equation, while magnetic effects have been integrated into the momentum equations. Blood has used as base fluid in which the nanoparticles of Cu and CuO have been mixed. Dimensionless variables have employed to transform the modeled equations facilitating their solution using bvp4c approach. In Section 1, the introduction is provided, followed by the problem formulation and methodology in Section 2. The methodology is discussed in Section 3. Section 4 presents the results of the study, and Section 5 concludes with the main findings.

2. Problem formulation

Let us examine the 3D flow of a Casson hybrid nanofluid over a surface extending in two directions. The motion in the fluid is induced by the stretching behavior of the sheet such that it stretches with a velocity $u_{\mathrm{w}} = cx$ in x direction while along y-axis its flow is given by $v_{\mathrm{w}} = bx$, where b, $c > 0$. The velocity slip constraints are executed in x and y directions. While B_0 is the strength of the magnetic field in z direction parallel to directions of fluid flow. Additionally, we assume that the sheet surface is heated by a hot working fluid with a heat transfer coefficient h_{f}. Furthermore, the fluid, surface, and free stream temperatures are illustrated by T_{f}, T_{w}, and T_∞, such that $T_{\mathrm{f}} > T_{\mathrm{w}} > T_\infty$ as depicted in Fig. 1.

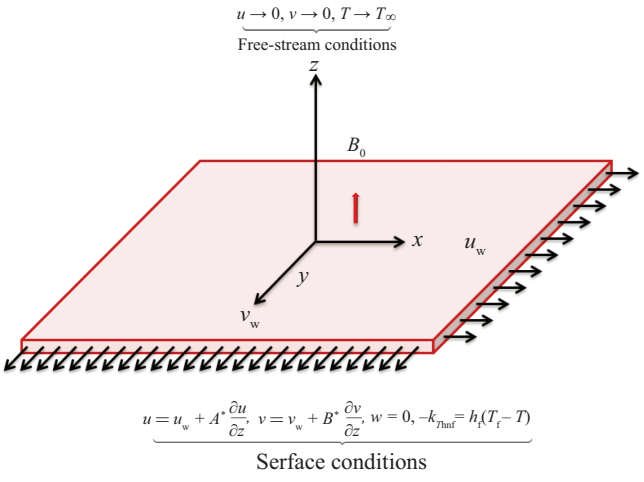


Fig. 1. Graphical view of flow pattern.

Considering these assumptions, we can express the fundamental equations of flow as follows:[41–43]

$$\frac{\partial u}{\partial x}+\frac{\partial v}{\partial y}+\frac{\partial w}{\partial z}=0, \tag{1}$$

$$u\frac{\partial u}{\partial x}+v\frac{\partial u}{\partial y}+w\frac{\partial u}{\partial z}=\frac{\mu_{\rm hnf}}{\rho_{\rm hnf}}\left(1+\frac{1}{\beta}\right)\frac{\partial^2 u}{\partial z^2}-\left(\frac{\sigma_{\rm hnf}B_0^2}{\rho_{\rm hnf}}+\frac{\mu_{\rm hnf}}{\rho_{\rm hnf}K(z)}\right)u, \tag{2}$$

$$u\frac{\partial v}{\partial x}+v\frac{\partial v}{\partial y}+w\frac{\partial v}{\partial z}=\frac{\mu_{\rm hnf}}{\rho_{\rm hnf}}\left(1+\frac{1}{\beta}\right)\frac{\partial^2 v}{\partial z^2}-\left(\frac{\sigma_{\rm hnf}B_0^2}{\rho_{\rm hnf}}+\frac{\mu_{\rm hnf}}{\rho_{\rm hnf}K(z)}\right)v, \tag{3}$$

$$u\frac{\partial T}{\partial x}+v\frac{\partial T}{\partial y}+w\frac{\partial T}{\partial z}=\frac{k_{\rm hnf}}{(\rho C_p)_{\rm hnf}}\frac{\partial^2 T}{\partial z^2}+\frac{16\sigma^* T_\infty^3}{3k^*(\rho C_p)_{\rm hnf}}\frac{\partial^2 T}{\partial z^2}+\frac{q_1}{(\rho c_p)_{\rm hnf}}(T-T_\infty)+\frac{q_2}{(\rho c_p)_{\rm hnf}}(T_{\rm f}-T_\infty)\exp(-a\eta). \tag{4}$$

The constraints at boundaries are

$$u=u_{\rm w}+A^*\frac{\partial u}{\partial z},\ v=v_{\rm w}+B^*\frac{\partial v}{\partial z},\ w=0,\ -k_{\rm hnf}=h_{\rm f}(T_{\rm f}-T)\ \text{at}\ z=0,\ u\to 0,\ v\to 0,\ T\to T_\infty\ \text{as}\ z\to\infty. \tag{5}$$

The similarity variables are defined as[41]

$$\eta=z\sqrt{\frac{c}{\upsilon_{\rm f}}},\quad u=cxf'(\eta),\quad v=cyg'(\eta),\quad T=T_\infty+(T_{\rm f}-T_\infty)\theta(\eta),\quad w=-\sqrt{c\upsilon_{\rm f}}(f(\eta)+g(\eta)). \tag{6}$$

Moreover, in the above equations,

$$K(z)=\frac{m^2\varepsilon(z)^3}{(1-\varepsilon(z))^2},\qquad \varepsilon(z)=\varepsilon_0\left(1+\varepsilon_1\exp\left(\frac{x\varepsilon_2}{m}\right)\right). \tag{7}$$

In Eq. (7), ε_1 and ε_2 are the empirical constants subject to porous particle diameter, ε_0 represents the ambient porosity, and m is the particle diameter as mentioned in Ref. [44]. Furthermore, the empirical constants and the diameter of porous particles are maintained at a constant level within the range $(0<m,\varepsilon_0,\varepsilon_1,\varepsilon_2<1)$ that is favorable for the flow field as shown in Ref. [44].

Incorporating Eq. (6) in Eqs. (1)–(4) we have

$$\left(1+\frac{1}{\beta}\right)f'''(\eta)-Q_1Q_2\left\{f'^2(\eta)-(f(\eta)+g(\eta))f''(\eta)\right\}-\left(Q_1Q_3M-\frac{1}{Da}\frac{\left[1-\varepsilon_0\left(1+\varepsilon_1\exp\left(-\varepsilon_2\eta/\sqrt{Da}\right)\right)\right]^2}{\left[\varepsilon_0^3\left(1+\varepsilon_1\exp\left(-\varepsilon_2\eta/\sqrt{Da}\right)\right)\right]^3}\right)f'(\eta)=0, \tag{8}$$

$$\left(1+\frac{1}{\beta}\right)g'''(\eta)-Q_1Q_2\left\{g'^2(\eta)-(f(\eta)+g(\eta))g''(\eta)\right\}-\left(Q_1Q_3M-\frac{1}{Da}\frac{\left[1-\varepsilon_0\left(1+\varepsilon_1\exp\left(-\varepsilon_2\eta/\sqrt{Da}\right)\right)\right]^2}{\left[\varepsilon_0^3\left(1+\varepsilon_1\exp\left(-\varepsilon_2\eta/\sqrt{Da}\right)\right)\right]^3}\right)g'(\eta)=0, \tag{9}$$

$$(Q_4+Rd)\theta''(\eta)+Q_5Pr(f(\eta)+g(\eta))\theta'(\eta)+PrQ_T\theta(\eta)+PrQ_S\exp(-a\eta)=0. \tag{10}$$

With subjected conditions at boundaries

$$\begin{aligned}&f'(\eta=0)=1+\alpha f''(\eta=0),\quad g'(\eta=0)=\beta_1+\gamma g''(\eta=0),\quad f(\eta=0)=0,\quad g(\eta=0)=0,\\&-k_{\rm Thnf}\theta'(\eta=0)=Bi(\theta(\eta=0)-1),\quad f'(\eta\to\infty)\to 0,\quad g'(\eta\to\infty)\to 0,\quad \theta(\eta\to\infty)\to 0.\end{aligned} \tag{11}$$

The dimensionless emerging factors are defined as follows with its physical description in nomenclature table:

$$\left\{\begin{aligned}&Q_1=\frac{\mu_{\rm f}}{\mu_{\rm hnf}},\quad Q_2=\frac{\rho_{\rm hnf}}{\rho_{\rm f}},\quad Q_3=\frac{\sigma_{\rm hnf}}{\sigma_{\rm f}},\quad Q_4=\frac{k_{\rm hnf}}{k_{\rm f}},\quad Q_5=\frac{(\rho C_p)_{\rm hnf}}{(\rho C_p)_{\rm f}},\quad Pr=\frac{(\mu_{\rm f}C_p)_{\rm f}}{k_{\rm f}},\quad Rd=\frac{16\sigma^*T_\infty^3}{3k^*k_{\rm f}},\quad \beta_1=\frac{b}{c},\\&Q_T=\frac{q_1}{c(\rho C_p)_{\rm f}},\quad Q_S=\frac{q_2}{c(\rho C_p)_{\rm f}},\quad Bi=\frac{h_{\rm f}}{k_{\rm f}}\sqrt{\frac{\upsilon_{\rm f}}{c}},\quad \alpha=A^*\sqrt{\frac{c}{\upsilon_{\rm f}}},\quad Da=\frac{\upsilon_{\rm f}}{\alpha m^2},\quad M=\frac{\sigma_{\rm f}B_0^2}{c\rho_{\rm f}},\quad \gamma=B^*\sqrt{\frac{c}{\upsilon_{\rm f}}}.\end{aligned}\right\} \tag{12}$$

2.1. Interested quantities

The skin frictions along x, y directions and local Nusselt number are defined as follows:

$$C_{\rm fx}=\frac{\tau_{{\rm w}x}}{\rho u_{\rm w}^2/2},\qquad C_{\rm fy}=\frac{\tau_{\rm wy}}{\rho u_{\rm w}^2/2},\qquad Nu_x=\frac{xq_{\rm w}}{k_{\rm f}(T_{\rm f}-T_\infty)}, \tag{13}$$

where $\tau_{{\rm w}x}$ and $\tau_{\rm wy}$ are the shear stresses along x and y directions, respectively, and $q_{\rm w}$ is the heat flux, mathematically these quantities are illustrated as

$$\tau_{{\rm w}x}=\mu_{\rm hnf}\left.\frac{\partial u}{\partial z}\right|_{z=0},\quad \tau_{\rm wy}=\mu_{\rm hnf}\left.\frac{\partial v}{\partial z}\right|_{z=0},\quad q_{\rm w}=-\left(k_{\rm hnf}+\frac{16T_\infty^3\sigma^*}{3k^*}\right)\left.\frac{\partial T}{\partial z}\right|_{z=0}. \tag{14}$$

Using similarity variables, equation (12) is reduced as

$$C_{\rm fx}Re_x^{1/2}=\frac{1}{Q_1}f''(0),\qquad C_{\rm fy}Re_y^{1/2}=\frac{1}{Q_1}g''(0),\qquad Nu_xRe_x^{-1/2}=-Q_4(1+Rd)\theta'(0). \tag{15}$$

2.2. Thermophysical properties of Cu–CuO/blood

In this study, a hybrid nanofluid is examined which characterized as a diluted colloidal blend of Cu–CuO nanoparticles suspended in blood, which serves as the working fluid. The thermophysical properties of both the nanoparticles and the active working fluid (blood) are described in Table 1. Moreover, in this work Cu/blood is unary nanofluid and Cu–CuO/blood is hybrid nanofluid. The correlations depicting the thermophysical and rheological characteristics of nanofluids are expressed as follows:

$$\frac{\mu_{\rm hnf}}{\mu_{\rm f}}=\frac{1}{(1-\varphi_1)^{2.5}(1-\varphi_2)^{2.5}},\quad \frac{\rho_{\rm hnf}}{\rho_{\rm f}}=(1-\varphi_1)\left\{1-\varphi_1+\varphi_1\left(\frac{\rho_{s1}}{\rho_{\rm f}}\right)\right\}+\varphi_2\left(\frac{\rho_{s2}}{\rho_{\rm f}}\right), \tag{16}$$

$$\frac{\sigma_{\rm hnf}}{\sigma_{\rm f}}=1+\frac{3\left(\dfrac{\sigma_1\varphi_1+\sigma_2\varphi_2}{\sigma_{\rm f}}-(\varphi_2+\varphi_1)\right)}{2+\left(\dfrac{\sigma_1\varphi_1+\sigma_2\varphi_2}{(\varphi_2+\varphi_1)\,\sigma_{\rm f}}\right)-\left(\dfrac{\sigma_1\varphi_1+\sigma_2\varphi_2}{\sigma_{\rm f}}-(\varphi_2+\varphi_1)\right)}, \tag{17}$$

$$\frac{(\rho c_p)_{\rm hnf}}{(\rho c_p)_{\rm f}}=(1-\varphi_2)\left\{1-\varphi_1+\varphi_1\left(\frac{(\rho c_p)_{s1}}{(\rho c_p)_{\rm f}}\right)\right\}+\varphi_2\left(\frac{(\rho c_p)_{s2}}{(\rho c_p)_{\rm f}}\right), \tag{18}$$

$$\frac{k_{\rm hnf}}{k_{\rm f}}=\frac{2k_{\rm nf}+k_{s2}-2(k_{\rm nf}-k_{s2})\varphi_2}{2k_{\rm nf}+k_{s2}+2(k_{\rm nf}-k_{s2})\varphi_2},\quad \frac{k_{\rm nf}}{k_{\rm f}}=\frac{2k_{\rm f}+k_{s1}-2(k_{\rm f}-k_{s1})\varphi_1}{2k_{\rm f}+k_{s1f}+(k_{\rm f}-k_{s1})\varphi_1}. \tag{19}$$

Table 1. Numerical features of blood Cu and CuO nanoparticles.

Property	Blood	Cu	CuO
ρ (kg·m^{-3})	1063	8933	6500
C_p (J·kg^{-1}·K^{-1})	3594	385	540
k (W·m^{-1}·K^{-1})	0.492	400	18
σ (S·m^{-1})	0.8	5.96×10^{7}	2.7×10^{-8}

3. Solution method

To solve Eqs. (8)–(10) using Eq. (11) we shall use bvp4c approach. It is a numerical method commonly used to solve ODEs. This method employs a fourth-order collocation technique to discretize the differential equation and then solves the resulting system of algebraic equations using iterative numerical methods. This method is particularly useful for nonlinear boundary value problems, including those arising in various fields such as physics, engineering, and mathematical modeling, offering a robust and efficient approach to obtaining numerical solutions for complex systems. For current problem this method is described as follows:

$$\begin{aligned}&f=\tau(1),\ f'=\tau(2),\ f''=\tau(3),\ f'''=\tau'(3),\\ &g=\tau(4),\ g'=\tau(5),\ g''=\tau(6),\ g'''=\tau'(6),\ \theta=\tau(7),\ \theta'=\tau(8),\ \theta''=\tau'(8),\end{aligned} \tag{20}$$

$$\tau'(3)=-\frac{\left\{-Q_1Q_2\left\{(\tau(2))^2-(\tau(1)+\tau(4))\,\tau(3)\right\}-\left(Q_1Q_3M-\dfrac{1}{Da}\dfrac{\left[1-\varepsilon_0\left(1+\varepsilon_1\exp\left(\dfrac{-\varepsilon_2\eta}{\sqrt{Da}}\right)\right)\right]^2}{\left[\varepsilon_0^3\left(1+\varepsilon_1\exp\left(\dfrac{-\varepsilon_2\eta}{\sqrt{Da}}\right)\right)\right]^3}\right)\tau(2)\right\}}{(1+1/\beta)}, \tag{21}$$

$$\tau'(6)=-\frac{\left\{-Q_1Q_2\left\{(\tau(5))^2-(\tau(1)+\tau(4))\,\tau(6)\right\}-\left(Q_1Q_3M-\dfrac{1}{Da}\dfrac{\left[1-\varepsilon_0\left(1+\varepsilon_1\exp\left(\dfrac{-\varepsilon_2\eta}{\sqrt{Da}}\right)\right)\right]^2}{\left[\varepsilon_0^3\left(1+\varepsilon_1\exp\left(\dfrac{-\varepsilon_2\eta}{\sqrt{Da}}\right)\right)\right]^3}\right)\tau(5)\right\}}{(1+1/\beta)}, \tag{22}$$

$$\tau'(8)=\left\{\frac{Q_5Pr\,(\tau(1)+\tau(4))\,\tau(8)+PrQ_T\tau(7)+\Pr\,Q_S\exp(-a\eta)}{(Q_4+Rd)}\right\}. \tag{23}$$

With subjected conditions at boundaries:

$$\begin{aligned}&\tau_a(1)-0,\ \ \tau_a(2)-1-\alpha\tau_a(3),\ \ \tau_b(2)-0,\ \ \tau_a(4)-0,\\ &\tau_a(5)-\beta_1-\gamma\tau_a(6),\ \ k_{\rm hnf}\tau_a(8)+Bi\,(\tau_a(7)-1),\ \ \tau_b(5)-0,\ \ \tau_b(7)-0.\end{aligned} \tag{24}$$

3.1. Validation

In order to verify the accuracy of current analysis, we have cross-referenced our findings with the existing data documented in Refs. [45–48]. This comparative examination ensures the reliability and validity of our results by confirming their consistency with previously established information. This validation is ensured in Table 2 with published literature for different values of Pr by ignoring all other factor, *i.e.*, by taking $Rd = 0$, β_1, $Q_T = 0$, $Q_S = 0$, $Bi = 0$, $\alpha = 0$, $Da = 0$, $M = 0$, $\gamma = 0$. Moreover, taking $Bi = 0$ suggests that the convective condition is to be eliminated and hence (Bi) is to be vanished.

Table 2. Validation of the present results with published literature for different values of Pr when all other embedding factors are ignored.

Pr	Khan and Pop[45]	Gorla and Sidawi[46]	Kouz & Owhaib[47]	Dawar *et al.*[48]	Present results
0.07	0.0663	0.0654	0.06562	0.01566480561	0.0656225831
0.2	0.1691	0.1691	0.16909	0.16908861990	0.1690886181
0.7	0.4539	0.5349	0.45392	0.45391742750	0.4539168161
2.0	0.9113	0.9114	0.91136	0.91136139280	0.9113613923
7.0	1.8954	1.8905	1.89542	1.89542020000	1.8954201990

4. Discussion of results

In this study blood-based hybrid nanofluid flow has considered on a convectively heated sheet. The sheet exhibits the properties of a variable porous medium and extends in both the x and y directions. Blood has used as base fluid in which the nanoparticles of Cu and CuO have been mixed. Thermal radiation, space-dependent, and thermal-dependent heat sources have been incorporated into the energy equation, while magnetic effects have been integrated into the momentum equations. Dimensionless variables have employed to transform the modeled equations facilitating their solution using bvp4c approach. The impacts of different emerging factors will be discussed in the following paragraphs.

4.1. Variations in flow profiles $f'(\eta)$ and $g'(\eta)$ and thermal profiles $\theta(\eta)$ *versus* Da

The impacts of variable porous space factor Da on velocity distributions $f'(\eta)$ and $g'(\eta)$ and thermal distribution $\theta(\eta)$ are depicted in Figs. 2(a)–2(c) by taking $Da = 1.0, 2.0, 5.0, 10.0$ while $Pr = 21$, $Rd = 1.0$, $Q_T = 1.5$, $Q_S = 1.5$, $Bi = 1.0$, $\alpha = 1.3$, $\beta_1 = 1.0$, $M = 2.5$, $\gamma = 1.3$. Figures 2(a) and 2(b) portray that an increase in Da with $Da = 1.0, 2.0, 5.0, 10.0$ results in a notable enhancement of both primary and secondary velocity distributions $f'(\eta)$ and $g'(\eta)$, particularly pronounced in Cu-blood nanofluid compared to Cu–CuO/blood hybrid nanofluid. Actually, on variable permeable bi-directional elongating surface, there is a greater enhancement in fluid flow characteristics when blood is mixed with copper nanoparticles. Physically, this can be explained as, to the unique properties of blood, such as its viscosity and red blood cell structure, which interacts differently with the variable porous medium compared to the hybrid nanofluid. Additionally, the presence of copper nanoparticles in blood leads to more effective fluid–particle interactions, resulting in a more significant augmentation of the velocity distributions within the variable porous medium as depicted in Figs. 2(a) and 2(b). This also suggests that within biological tissues as well as medical devices containing porous structures, the presence of blood combined with copper nanoparticles significantly alters fluid dynamics, leading to more efficient fluid flow. This finding holds crucial implications in medical sciences, especially in applications like drug delivery systems, where optimizing fluid flow within variable porous matrices is essential for ensuring effective transport of therapeutic agents to targeted tissues or organs. Figure 2(c) demonstrates that the escalation in Da with $Da = 1.0, 2.0, 5.0, 10.0$ leads to a notable reduction in $\theta(\eta)$. The observed decline in $\theta(\eta)$ with growth in Da influencing thermal distribution signifies a complex interaction between fluid flow characteristics and material properties. In the context of a bi-directional stretching sheet, the escalation in Da suggests a decrease in the effective variable porosity available for fluid passage on the surface o elongating sheet, thus limiting convective heat transfer. The more pronounced reduction observed with Cu-blood nanofluid compared to Cu–CuO/blood hybrid nanofluid implies that the addition of blood particles alters the fluid dynamics in a manner that impedes heat transfer more significantly. This could be endorsed to the unique rheological properties of blood nanoparticles, which may lead to increased viscosity and altered flow patterns, hindering the convective transport of heat along the stretching sheet. In the context of medical applications, such as in biomedical engineering or thermoregulation in biological systems, this finding implies that the presence of blood combined with copper nanoparticles in porous matrices significantly modifies thermal conduction and dissipation.

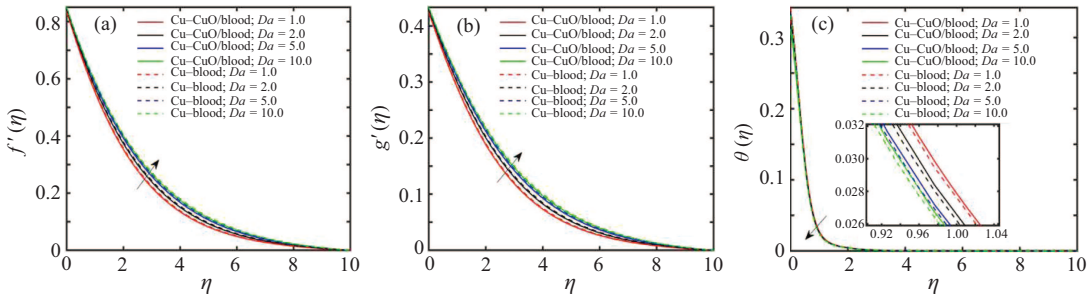


Fig. 2. Variations in $f'(\eta)$ and $g'(\eta)$ and thermal profiles $\theta(\eta)$ *versus* Da.

4.2. Variations in flow profiles $f'(\eta)$ and $g'(\eta)$ and thermal profiles $\theta(\eta)$ *versus* β_1

The impacts of stretching ratio factor β_1 on velocity distributions $f'(\eta)$ and $g'(\eta)$ and thermal distribution $\theta(\eta)$ have depicted in Figs. 3(a)–3(c) by taking $\beta_1 = 0.1, 0.2, 0.3, 0.4$ while $Pr = 21$, $Rd = 1.0$, $Q_T = 1.5$, $Q_S = 1.5$, $Bi = 1.0$, $\alpha = 1.3$, $Da = 1.0$, $M = 2.5$, $\gamma = 1.3$. From Fig. 3(a) it has observed that the profiles of $f'(\eta)$ are declining with escalation in β_1. The observed increase in stretching factor leads to a complex alteration in fluid flow dynamics, particularly in the distribution of primary and secondary velocities. As the stretching factor grows, it exerts a restraining effect on primary velocity distribution, likely due to enhanced drag forces experienced by the fluid. This results in a decrease in the flow velocity along the stretching direction. Conversely, the secondary velocity distribution experiences an upsurge, indicating an increase in transverse flow components perpendicular to the stretching direction. These changes are notably more pronounced in Cu-blood nanofluid compared to Cu–CuO/blood hybrid nanofluid, suggesting that the introduction of blood particles modifies the fluid's rheological properties as portrayed in Figs. 3(a) and 3(b). Figure 3(c) examines that growth β_1 decelerate the thermal flow distribution when fluid flows on an elongating variable surface in x and y directions. The observed decline in thermal distribution with increasing stretching factor indicates a complex relationship between fluid flow dynamics and heat transfer mechanisms on a bi-directional stretching sheet. As β_1 grows, it exerts a restraining influence on the fluid flow, potentially reducing the convective transport of heat across the sheet. This reduction in thermal distribution is more pronounced in the case of Cu-blood nanofluid in comparison of Cu–CuO/blood hybrid nanofluid, suggesting that the presence of blood particles alters the fluid's convective heat transfer properties. This phenomenon is associated with changes in the fluid's viscosity and thermal boundary layer characteristics induced by the blood nanoparticles, leading to a more significant impediment to heat transfer.

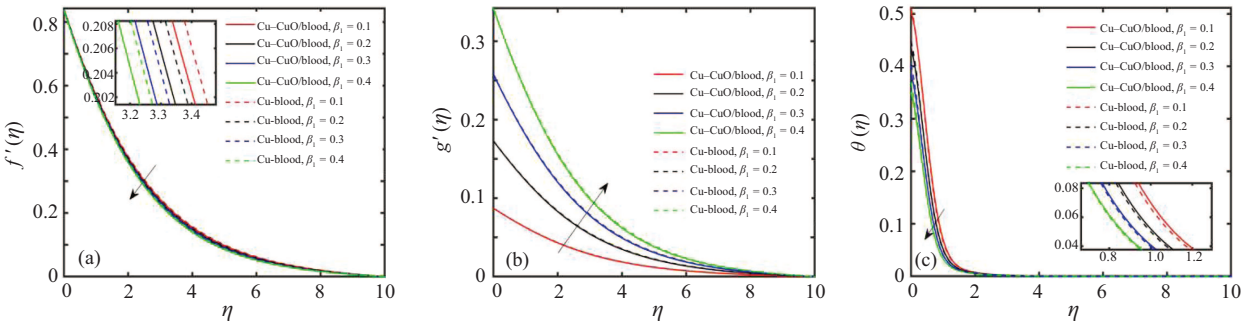


Fig. 3. Variations in $f'(\eta)$ and $g'(\eta)$ and thermal profiles $\theta(\eta)$ *versus* β_1.

4.3. Variations in flow profiles $f'(\eta)$ and $g'(\eta)$ and thermal profiles $\theta(\eta)$ *versus* β

The impacts of Casson factor β on velocity distributions $f'(\eta)$ and $g'(\eta)$ and thermal distribution $\theta(\eta)$ have depicted in Figs. 4(a)–4(c) by taking $\beta = 1.0, 2.0, 3.0, 4.0$ while $Pr = 21$, $Rd = 1.0$, $Q_T = 1.5$, $Q_S = 1.5$, $Bi = 1.0$, $\beta_1 = 1.0$, $\alpha = 1.3$, $Da = 1.0$, $M = 2.5$, $\gamma = 1.3$. The increase in the Casson factor, that characterizes the non-Newtonian behavior of fluids, results in a retardation of both primary and secondary velocity distributions $f'(\eta)$ and $g'(\eta)$ as depicted in Figs. 4(a) and 4(b). This phenomenon is particularly pronounced Cu–CuO/blood hybrid nanofluid. Physically, this can be explained as, the Casson factor increases, the fluid's resistance to flow also increases due to enhanced internal friction and cohesion between the nanoparticles and the base fluid. Consequently, the fluid particles require more energy to overcome this in-

creased resistance, leading to a reduction in the fluid's velocity and a delay in the establishment of the primary and secondary velocity profiles. In the case of Cu–CuO/blood hybrid nanofluid, the presence of nanoparticles further amplifies these effects due to their higher density and larger surface area, exacerbating the retardation of velocity distributions compared to traditional fluids as depicted in Figs. 4(a) and 4(b). In contrast, with upsurge in β by taking $\beta = 1.0, 2.0, 3.0, 4.0$, while $Pr = 21$, $Rd = 1.0$, $Q_T = 1.5$, $Q_S = 1.5$, $Bi = 1.0$, $\beta_1 = 1.0$, $\alpha = 1.3$, $Da = 1.0$, $M = 2.5$, $\gamma = 1.3$, there is an escalation in thermal panels $\theta(\eta)$ as described in Fig. 4(c). Actually, an increase in β results in heightened fluid viscosity and internal cohesion due to stronger interactions between the nanoparticles and the base fluid. Consequently, the fluid's ability to carry and disperse heat improves, leading to an augmentation in $\theta(\eta)$. In case of Cu–CuO/blood hybrid nanofluid, the presence of nanoparticles amplifies this effect due to their higher density and larger surface area, facilitating more efficient heat transfer compared to Cu–blood nanofluid. Therefore, the growth in β induces a more significant enhancement in thermal distribution, particularly pronounced in Cu–CuO/blood hybrid nanofluid systems with increased nanoparticle concentrations and altered material characteristics.

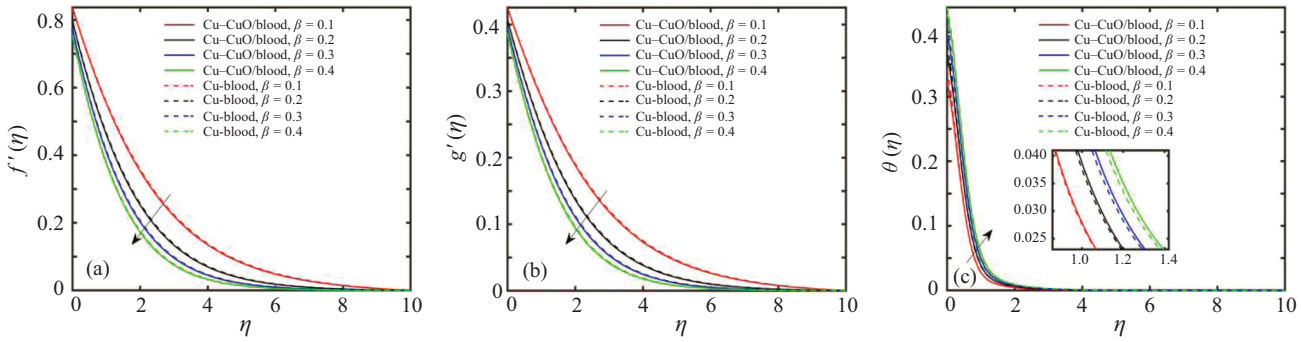


Fig. 4. Variations in $f'(\eta)$ and $g'(\eta)$ and thermal profiles $\theta(\eta)$ *versus* β.

4.4. Variations in flow profiles $f'(\eta)$ and $g'(\eta)$ and thermal profiles $\theta(\eta)$ *versus* M

The impacts of magnetic factor M on velocity distributions $f'(\eta)$ and $g'(\eta)$ and thermal distribution $\theta(\eta)$ have portrayed in Figs. 5(a)–5(c) by taking $M = 1.0, 2.0, 3.0, 4.0$ while $Pr = 21$, $Rd = 1.0$, $Q_T = 1.5$, $Q_S = 1.5$, $Bi = 1.0$, $\beta_1 = 1.0$, $\alpha = 1.3$, $Da = 1.0$, $\beta = 1.0$, $\gamma = 1.3$. The increase in M, that offers resistance to fluid motion on the sheet's surface, results in a retardation of both primary and secondary velocity distributions $f'(\eta)$ and $g'(\eta)$ as shown in Figs. 5(a) and 5(b).

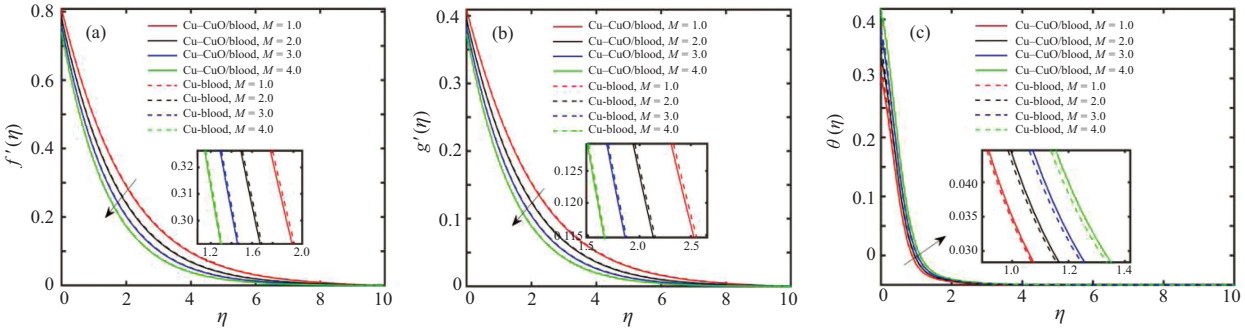


Fig. 5. Variations in $f'(\eta)$ and $g'(\eta)$ and thermal profiles $\theta(\eta)$ *versus* M.

Physically, when M augments on the surface of sheet, the magnetic field strength intensifies, inducing stronger Lorentz forces within the fluid. These forces act to dampen fluid motion, thereby reducing the velocity distributions $f'(\eta)$ and $g'(\eta)$. In the case of hybrid nanofluids containing Cu–CuO/blood, the presence of magnetic nanoparticles exacerbates this effect due to their higher susceptibility to magnetic fields, resulting in a more pronounced reduction in velocity distributions compared to Cu-blood nanofluid. Therefore, the growth in magnetic factor induces a more significant decrease in both primary and secondary velocity distributions, particularly evident in hybrid nanofluid systems with increased nanoparticle concentrations and altered material properties as depicted in Figs. 5(a) and 5(b). In contrast, with upsurge in M by taking $M = 1.0, 2.0, 3.0, 4.0$ while $Pr = 21$, $Rd = 1.0$, $Q_T = 1.5$, $Q_S = 1.5$, $Bi = 1.0$, $\beta_1 = 1.0$, $\alpha = 1.3$, $Da = 1.0$, $\beta = 2.5$, $\gamma = 1.3$, there is an escalation in thermal panels $\theta(\eta)$ as described in Fig. 5(c). This can be interpreted physically

as M grows; the applied magnetic field strengthens, leading to enhanced MHD effects within the fluid on the porous surface with variable features on bi-directional sheet. These effects result in increased fluid motion and mixing, which in turn improves heat transfer throughout the system. In the case of Cu–CuO/blood hybrid nanofluids, the presence of magnetic nanoparticles further amplifies this phenomenon due to their higher susceptibility to magnetic fields, resulting in a more significant enhancement of thermal distribution compared to pure copper nanofluids. Thus, the growth in M induces a more pronounced augmentation in $\theta(\eta)$, particularly evident in case of hybrid nanofluid as depicted in Fig. 5(c).

4.5. Variations in flow profiles $f'(\eta)$ *versus* α

Figure 6 depicts the impact of slip factor α along x direction in primary velocity distribution $f'(\eta)$ by taking by taking $\alpha = 0.1, 0.3, 0.5, 0.7$ while $Da = 1.0$, $\beta = 2.5$, $\gamma = 1.3$, $M = 1$, $Pr = 21$, $Rd = 1.0$, $Q_T = 1.5$, $Q_S = 1.5$, $Bi = 1.0$, $\beta_1 = 1.0$. It is evident in this figure that with growth α there is reduction in $f'(\eta)$ which is more significant in case of Cu–CuO/blood hybrid nanofluid in comparison of Cu-blood nanofluid.

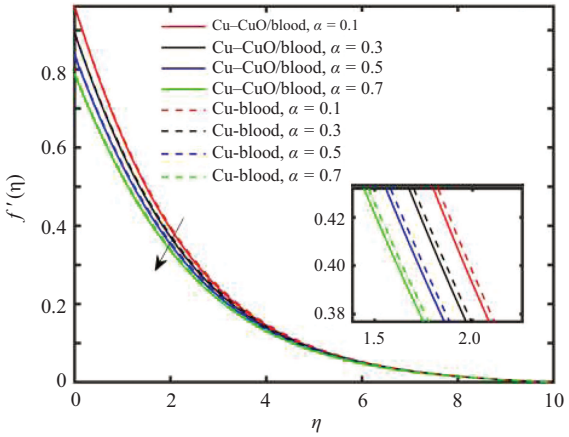


Fig. 6. Variations in $f'(\eta)$ *versus* α.

Physically, as α increases, the slip velocity between the fluid and the surface along the x-axis becomes more significant, effectively decreasing the fluid velocity near the boundary. In the case of Cu–CuO/blood hybrid nanofluid, the presence of nanoparticles exacerbates this effect due to increased interactions with the sheet's surface and altered fluid-solid interface characteristics. Consequently, the reduction in $f'(\eta)$ is more pronounced in hybrid nanofluids compared to pure copper nanofluids. Therefore, the growth in α along the x-axis induces a more significant decrease in $f'(\eta)$, particularly evident in Cu–CuO/blood hybrid nanofluid.

4.6. Variations in flow profiles $g'(\eta)$ *versus* γ

Figure 7 depicts the impact of slip factor γ along y direction in primary velocity distribution $g'(\eta)$ by taking $\gamma = 0.1, 0.3, 0.5, 0.7$ while $Da = 1.0$, $\beta = 2.5$, $\alpha = 1.3$, $Bi = 1.0$, $\beta_1 = 1.0$. $M = 1$, $Pr = 21$, $Rd = 1.0$, $Q_T = 1.5$, $Q_S = 1.5$.

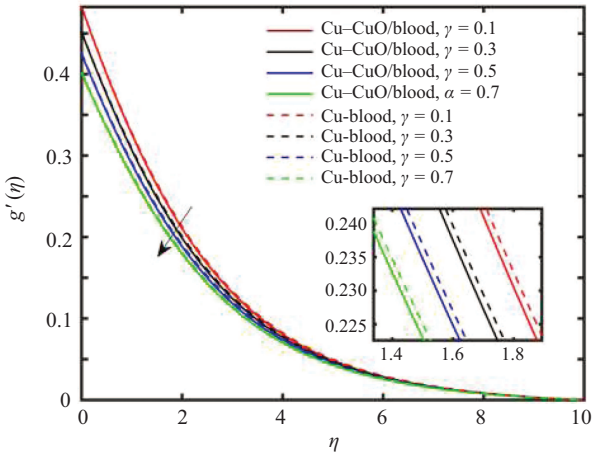


Fig. 7. Variations in $g'(\eta)$ *versus* γ.

It is evident in this figure that with growth γ there is reduction in $f'(\eta)$ which is more significant in case of Cu–CuO/blood hybrid nanofluid in comparison of Cu-blood nanofluid. This phenomenon can be interpreted physically as the slip factor describes the relative motion between the fluid and the surface of bi-directional geometry, affecting the momentum transfer within the fluid. As γ expands, the momentum transfer becomes more efficient, diminishing the formation and intensity of secondary flows. In the case of Cu–CuO/blood hybrid nanofluid, the presence of blood constituents alters the fluid dynamics, enhancing the slip effect further due to potential changes in viscosity and surface properties. This intensified slip effect consequently suppresses secondary velocity distribution to a greater extent in hybrid nanofluids compared to their pure copper counterparts, highlighting the complex interaction between fluid properties and slip phenomena in nanofluid dynamics.

4.7. Variations in thermal profiles $\theta(\eta)$ *versus* Q_S, Q_T, and Bi

Figures 8(a)–8(c) depict the impact of space-dependent heat source Q_S, thermal-dependent heat source and thermal Biot number on thermal distribution $\theta(\eta)$. The impacts of Q_S on $\theta(\eta)$ is depicted in Fig. 8(a) with $Q_S = 0.1, 0.3, 0.5, 0.7$ while $Da = 1.0$, $\beta = 2.5$, $\alpha = 1.3$, $Bi = 1.0$, $\beta_1 = 1.0$, $M = 1$, $Pr = 21$, $Rd = 1.0$, $Q_T = 1.5$, $\gamma = 1.3$. It has noticed in this graphical view that $\theta(\eta)$ is escalating with upsurge in Q_S. This phenomenon can be understood physically as a growth in Q_S contributes additional heat to the fluid flowing on the surface of variable porous media, thereby increasing the overall thermal energy within the system. In the case of hybrid nanofluids containing blood constituents, the presence of additional heat enhances the thermal conductivity and convective heat transfer properties of the fluid, facilitating more efficient heat dissipation and distribution on the stretching sheet's

surface. Consequently, the escalation in $\theta(\eta)$ becomes more pronounced for Cu–CuO/blood hybrid nanofluid in comparison of Cu-blood nanofluid due to the combined effects of enhanced thermal properties and the influence of blood constituents. Figure 8(b) depicts the impact of thermal-dependent heat source Q_T, on $\theta(\eta)$ taking $Q_T = 0.1, 0.3, 0.5, 0.7$ while $Pr = 21$, $Rd = 1.0$, $Q_S = 1.5$, $\gamma = 1.3$, $Bi = 1.0$, $\beta_1 = 1.0$, $\beta = 2.5$, $\alpha = 1.3$, $M = 1$, $Da = 1.0$. It has noticed in this graphical view that $\theta(\eta)$ is escalating with upsurge in Q_T with a more pronounced effect observed for Cu–CuO/blood hybrid nanofluid in comparison of Cu-blood nanofluid for fluid flow over a bi-directional stretching sheet. This phenomenon can be interpreted as the combined result of enhanced thermal conductivity and convective heat transfer properties of the nanofluid mixture, particularly evident in the presence of copper oxide nanoparticles. The inclusion of blood as a dispersing medium further influences the heat transfer characteristics due to its unique rheological properties, potentially leading to increased convective heat transfer rates. Hence growth in Q_T results escalation in thermal profiles $\theta(\eta)$ for fluid flows on bidirectional elongating sheet.

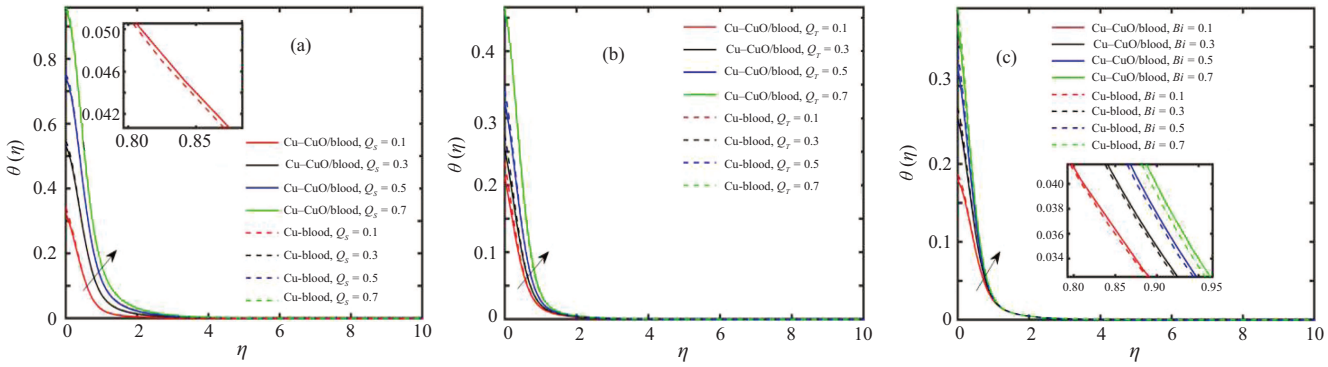


Fig. 8. Variations in $\theta(\eta)$ *versus* Q_S, Q_T, and Bi.

Figure 8(c) portrays the impact of thermal Biot number Bi, on $\theta(\eta)$ taking $Bi = 0.1, 0.3, 0.5, 0.7$ while $Pr = 21$, $Rd = 1.0$, $Q_S = 1.5$, $\gamma = 1.3$, $Q_T = 1.5$, $\beta_1 = 1.0$, $Da = 1.0$, $\beta = 2.5$, $\alpha = 1.3$, $M = 1$. It has noticed in this figure that $\theta(\eta)$ is escalating with upsurge in Bi with a more significant effect noticed in case of Cu–CuO/blood hybrid nanofluid in comparison of Cu-blood nanofluid for fluid flow over a variable porous stretching sheet. Physically, growth in Bi indicates a strengthening of the thermal resistance at the fluid-stretching sheet interface, suggesting that heat transfer from the sheet's surface to the surrounding fluid is less efficient relative to internal thermal conduction within the fluid. Consequently, as Bi grows the width of thermal layer at boundary impeding the dissipation of heat into the fluid and resulting in a more significant buildup of thermal energy near the stretching surface. This phenomenon intensifies the temperature gradient across the boundary layer and amplifies the thermal distribution along the bi-directional stretching sheet, influencing heat transfer characteristics and overall thermal behavior within the fluid flow system.

4.8. Discussion of tables

The thermophysical properties of both the nanoparticles and the active working fluid (blood) are described in Table 1. Table 2 depicts the variations in $C_{fx}Re_x^{1/2}$ for different values of magnetic factor M, Casson factor β, stretching ratio factor β_1, variable porous space factor Da and slip factors α and γ respectively along x- and y-axes. It has observed from this table the skin friction $C_{fx}Re_x^{1/2}$ augments with upsurge in M, β, and β with more retardation in case of Cu-nanoparticles in comparison of Cu + CuO-nanoparticles. The magnetic field induces resistance in the motion of nanoparticles, impeding fluid flow and resulting in higher $C_{fx}Re_x^{1/2}$ along x-axis. Increased Casson factor signifies greater fluid viscosity, which leads to enhanced resistance to flow and elevated $C_{fx}Re_x^{1/2}$. Additionally, higher stretching ratio factors indicate greater stretching and deformation of the fluid, which intensifies fluid drag and further elevate skin friction. Copper nanoparticles, due to their higher conductivity, experiences more significant magnetic interactions, leading to greater disturbances in fluid flow and consequently higher skin friction compared to copper oxide nanoparticles. It has also noticed in Table 2 that $C_{fx}Re_x^{1/2}$ decelerates with upsurge in Da, α, and γ. Actually, the variable porous factor introduces additional pathways for fluid flow through the porous medium, allowing for more efficient dissipation of momentum and reducing skin friction $C_{fx}Re_x^{1/2}$. Slip factors along the x- and y-axes facilitate easier movement of the fluid adjacent to the stretching sheet, decreasing the resistance to flow and further diminishing skin friction $C_{fx}Re_x^{1/2}$. Copper nanoparticles, being more conductive, exhibits stronger interactions with the slip conditions and porous medium, leading to more substantial alterations in fluid dynamics compared to copper oxide nanoparticles.

Table 2. Behavior of skin friction $C_{fx}Re_x^{1/2}$ along x-axis for variation in different factors regarding Cu-blood nanofluid and Cu–CuO/blood hybrid nanofluid.

M	β	β_1	Da	α	γ	$C_{fx}Re_x^{1/2}$	
						Cu-blood	Cu–CuO/blood
0.1						–0.2932449301	–0.2665723196
0.3						–0.3060900489	–0.2780165263
0.5						–0.3182654604	–0.2888721300
0.7						–0.3298355735	–0.2991948452
	0.1					–0.2932449301	–0.2665723196
	0.3					–0.4087104920	–0.3712834604
	0.5					–0.4617364451	–0.4192939471
	0.7					–0.4939846251	–0.4484689722
		0.1				–0.2833386664	–0.2574580474
		0.3				–0.2884304898	–0.2621459218
		0.5				–0.2932449301	–0.2665723196
		0.7				–0.2978274328	–0.2707809785
			1.0			–0.2932449301	–0.2665723196
			2.0			–0.2826055463	–0.2572273107
			3.0			–0.2777512934	–0.2529737141
			4.0			–0.2749996449	–0.2505655107
				1.0		–0.2453577930	–0.2225833649
				2.0		–0.1869226074	–0.1691680090
				3.0		–0.1519928654	–0.1373678436
				4.0		–0.1285057133	–0.1160365999
					1.0	–0.2917364320	–0.2651744193
					2.0	–0.2896686404	–0.2632639692
					3.0	–0.2882941187	–0.2619971304
					4.0	–0.2873031060	–0.2610850520

Table 3. Behavior of skin friction $C_{fy}Re_y^{1/2}$ along y-axis for variation in different factors regarding Cu-blood nanofluid and Cu–CuO/blood hybrid nanofluid.

M	β	β_1	Da	α	γ	$C_{fy}Re_y^{1/2}$	
						Cu-blood	Cu–CuO/blood
0.1						–0.1345916718	–0.1222218800
0.3						–0.1418778957	–0.1287294968
0.5						–0.1487180229	–0.1348428375
0.7						–0.1551637234	–0.1406070422
	0.1					–0.1345916718	–0.1222218800
	0.3					–0.1882876897	–0.1709097026
	0.5					–0.2132204092	–0.1934865164
	0.7					–0.2284703780	–0.2072862642
		0.1				–0.0233741848	–0.0211704494
		0.3				–0.0757568561	–0.0687233938
		0.5				–0.1345916718	–0.1222218800
		0.7				–0.1989409525	–0.1807844698
			1.0			–0.1345916718	–0.1222218800
			2.0			–0.1282342702	–0.1166193799
			3.0			–0.1252757133	–0.1140185347
			4.0			–0.1235807904	–0.1125305438
				1.0		–0.1328640929	–0.1206174788
				2.0		–0.1305632574	–0.1184876632
				3.0		–0.1290590721	–0.1170987260
				4.0		–0.1279793006	–0.1161030158
					1.0	–0.1151888383	–0.1044288031
					2.0	–0.0900272053	–0.0814513376
					3.0	–0.0742216218	–0.0670696501
					4.0	–0.0632830273	–0.0571385404

An analogous behavior has noticed in Table 3 regarding the skin friction $C_{fy}Re_y^{1/2}$ along y-axis for different values of magnetic factor M, Casson factor β, stretching ratio factor β_1, variable porous space factor Da, and slip factors α and γ respectively along x- and y-axes.

Table 4 depicts the variations in Nusselt number $Nu_xRe_x^{-1/2}$ for different values of space and thermal-dependent heat source factors Q_S and Q_T, magnetic factor M, variable porous space factor Da, and thermal Biot number Bi with an augmenting behavior $Nu_xRe_x^{-1/2}$ for growth in all the stated factors. Greater space and thermal-dependent heat source factors indicate increased heat generation within the fluid, promoting convective heat transfer and enhancing $Nu_xRe_x^{-1/2}$. The magnetic field influences the alignment and motion of nanoparticles, augmenting convective heat transfer and further elevating $Nu_xRe_x^{-1/2}$. Variable porous space allows for additional convective pathways, facilitating heat transfer and boosting $Nu_xRe_x^{-1/2}$. Moreover, higher thermal Biot numbers imply more significant thermal gradients at the nanoparticle-fluid interface, leading to enhanced heat transfer and an increased $Nu_xRe_x^{-1/2}$. Cu + CuO-nanoparticles, being more conductive, and exhibits stronger interactions with these factors, resulting in more pronounced enhancements in convective heat transfer and higher Nusselt numbers compared to copper nanoparticles.

Table 4. Behavior of Nusselt number $Nu_xRe_x^{-1/2}$ for variation in different factors regarding Cu-blood nanofluid and Cu–CuO/blood hybrid nanofluid.

Q_T	Q_S	M	Da	Bi	$Nu_xRe_x^{-1/2}$	
					Cu-blood	Cu–CuO/blood
0.1					0.6176937774	0.6440623822
0.2					0.6433695580	0.6710388193
0.3					0.6633865867	0.6924561918
0.4					0.6794270559	0.7098725476
	0.1				0.3148152800	0.3237902779
	0.2				0.4044090712	0.4188795410
	0.3				0.4940030035	0.5139688582
	0.4				0.5835969384	0.6090578796
		0.1			0.5754739919	0.6006238032
		0.3			0.5781833502	0.6034312029
		0.5			0.5808906699	0.6062421671
		0.7			0.5835969384	0.6090578796
			1.0		0.5835969384	0.6090578796
			2.0		0.5882946098	0.6140036334
			3.0		0.5903656926	0.6161930288
			4.0		0.5915191048	0.6174148850
				0.1	0.1416197417	0.1507054958
				0.2	0.2688989024	0.2845373215
				0.3	0.3839085930	0.4041799231
				0.4	0.4883428255	0.5117760628

5. Conclusions

In current study blood based-hybrid nanofluid flow has considered on a convectively heated sheet. The sheet exhibits the properties of a variable porous medium and extends in both the x and y directions. Blood has used as base fluid in which the nanoparticles of Cu and CuO have been mixed. Thermal radiation, space-dependent, and thermal-dependent heat sources have been incorporated into the energy equation, while magnetic effects have been integrated into the momentum equations. Dimensionless variables have employed to transform the modeled equations facilitating their solution using bvp4c approach. The impacts of different factors have been evaluated on different flow distributions. After detail insight of the work it has concluded the following points.

(i) The findings of this investigation have been compared with the existing literature, revealing a strong agreement among present and established results that ensured the validation of the model and method used in this work.

(ii) Growth in variable porous factor has augmented the primary and secondary velocities and declined the thermal distribution with significant impacts in case of Cu-blood nanofluid.

(iii) Escalation in stretching ratio factor has declined the primary velocity and thermal distribution while augmented the secondary velocity distribution with significant impacts in case of Cu-blood nanofluid.

(iv) Upsurge in Casson factor has retarded the primary and secondary velocities and augmented the thermal distribution with substantial impacts in case of Cu–CuO/blood hybrid nanofluid.

(v) Escalation in magnetic factor has retarded the primary and secondary velocities while magnified the thermal distribution with significant impacts in case of Cu–CuO/blood hybrid nanofluid.

(vi) Both the primary and secondary velocities have retarded with growth in slip factors along x- and y-axes.

(vii) Thermal distribution has escalated with growth in thermal and space-dependent factors as well as with augmentation in thermal Biot number.

(viii) The skin frictions $C_{fx}Re_x^{1/2}$ and $C_{fy}Re_y^{1/2}$ have escalated for upsurge in M, β, and β_1 with more retardation in case of Cu-nanoparticles in comparison of Cu + CuO-nanoparticles. Moreover, growth in in Da, α, and γ has declined both of the skin frictions $C_{fx}Re_x^{1/2}$ and $C_{fy}Re_y^{1/2}$.

(ix) Nusselt number $Nu_xRe_x^{-1/2}$ has augmented with growth space and thermal-dependent heat source factors Q_S and Q_T, magnetic factor M, variable porous space factor Da, and thermal Biot number Bi with more significant impacts in case of Cu-CuO/blood hybrid nanofluid.

(x) The embedded factors exert a more significant effects on the temperature of the hybrid nanofluid flow (Cu–CuO/blood) compared to the (Cu-blood) nanofluid.

Acknowledgement

This study is supported via funding from Prince Sattam bin Abdulaziz University (Grant No. PSAU/2024/R/1446).

References

[1] Mahian O, Kolsi L, Amani M, Estellé P, Ahmadi G, Kleinstreuer C and Pop I 2019 *Phys. Rep.* **790** 1
[2] Islam S, Khan A, Kumam P, Alrabaiah H, Shah Z, Khan W and Jawad M 2020 *Sci. Rep.* **10** 17823
[3] Acharya N, Mabood F, Shahzad S A and Badruddin I A 2022 *Int. Commun. Heat Mass Transfer* **130** 105781
[4] Varun Kumar R S, Gunderi Dhananjaya P, Naveen Kumar R, Punith Gowda R J and Prasannakumara B C 2022 *Int. J. Comput. Methods* **23** 12
[5] Bhatti M M, Arain M B, Zeeshan A, Ellahi, R and Doranehgard M H 2022 *J. Energy Storage* **45** 103511
[6] Algehyne E A, Alamrani F M, Khan A, Khan K A, Lone S A and Saeed A 2023 *Colloid Polym. Sci.* 1–14
[7] Chu Y M, Bashir S, Ramzan M and Malik M Y 2023 *Math. Methods Appl. Sci.* **46** 11568
[8] Eid M R and Nafe M A 2022 *Waves Random Complex Media* **32** 1103
[9] Waqas H, Farooq U, Liu D, Abid M, Imran M and Muhammad T 2022 *Int. Commun. Heat Mass Transfer* **138** 106303
[10] Nasir S, Sirisubtawee S, Juntharee P, Berrouk A S, Mukhtar S and Gul T 2022 *Appl. Nanosci.* **12** 2777
[11] Guedri K, Khan A, Sene N, Raizah, Z, Saeed A and Galal A M 2022 *Math. Probl. Eng.* **1** 3429439
[12] Guedri K, Khan A, Gul T, Mukhtar S, Alghamdi W, Yassen M F and Tag Eldin E 2022 *ACS Omega.* **7** 33432
[13] Alharbi K A M, Ahmed A E S, Ould Sidi M, Ahammad N A, Mohamed A, El-Shorbagy M A and Marzouki R 2022 *Micromachines* **13** 588
[14] Necib N, Benkhedda M, Tayebi T and Boufendi T 2024 *J. Therm. Anal. Calorim.* **149** 813
[15] Cao W, Animasaun I L, Yook S J, Oladipupo V A and Ji X 2022 *Int. Commun. Heat Mass Transfer* **135** 106069
[16] Shahzad H, Wang X, Ghaffari A, Iqbal K, Hafeez M B, Krawczuk M and Wojnicz W 2022 *Sci. Rep.* **12** 12219
[17] Shah I A, Bilal S, Asjad M I and Tag-ElDin E M 2022 *Micromachines* **13** 1624
[18] Khan U, Mebarek-Oudina F, Zaib A, Ishak A, Abu Bakar S, Sherif E S M and Baleanu D 2022 *Waves Random Complex Media* 1–14
[19] Gnanaprasanna K and Singh A K 2022 *Heat Transfer* **51** 6782
[20] Saleem M and Tufail M N 2023 *Phys. Scr.* **98** 095251
[21] Khan A, Saeed A, Gul T, Mukhtar S, Ali I and Jawad M 2021 *Phys. Scr.* **96** 045206
[22] Rasheed H U, Islam S, Zeeshan Khan, W Khan J and Abbas T 2022 *Adv. Mech. Eng.* **14** 16878132221085429
[23] Bejawada S G, Reddy Y D, Jamshed W, Nisar K S, Alharbi A N and Chouikh R 2022 *Alex. Eng. J.* **61** 8207
[24] Vishalakshi A B, Maranna T, Mahabaleshwar U S and Laroze D 2022 *Appl. Sci.* **12** 4937
[25] Mopuri O, Kodi R, Ganteda C, Srikakulapu R and Lorenzini G 2022 *J. Adv. Res. Fluid Mech. Therm. Sci.* **89** 62
[26] Reza-E-Rabbi S, Ahmmed S F, Islam S, Arifuzzaman S M, Rana B M J, Ali M Y and Khan M S 2022 2022 *Heat Transfer* **51** 6578
[27] Singh J K, Hanumantha and Seth G S 2022 *Heat Transfer* **51** 7613
[28] Abbas A, Jeelani M B, Alnahdi A S and Ilyas A 2022 *Processes* **10** 1221
[29] Santos-Moreno M, Valencia-Negrete C V and Fernandez-Anaya G 2022 *Fractals* **30** 2250178

[30] Hussain M, Farooq U and Sheremet M 2023 *Numer. Heat Transfer B: Fundam.* 1
[31] Yadav P K, Jaiswal S, Verma A K and Chamkha A J 2023 *J. Pet. Sci. Eng.* **220** 111113
[32] Soltanmohammadi R, Iraji S, de Almeida T R, Basso M, Munoz E R and Vidal A C 2024 *Energy Geosci.* **5** 100222
[33] Wahid N S, Arifin N M, Khashi'ie N S and Pop I 2023 *Chin. J. Phys.* **85** 196
[34] Choudhary P and Ray R K 2023 *Heat Transfer* **52** 4547
[35] Mondal P and Maiti D K 2023 *J. Eng. Thermophys.* **32** 835
[36] Mahmood Z, Khan U and Al-Zubaidi A 2023 *J. Therm. Anal. Calorim.* 1
[37] Reddy Y D, Goud B S, Nisar K S, Alshahrani B, Mahmoud M and Park C 2023 *Alex. Eng. J.* **64** 659
[38] Sharma B K, Kumar A, Gandhi R and Bhatti M M 2022 *Int. J. Mod. Phys. B* **36** 2250220
[39] Zaydan M, Hamad N H, Wakif A, Dawar A and Sehaqui R 2022 *Heat Transfer* **51** 2063
[40] Varun Kumar R S, Saleh B, Sowmya G, Afzal A, Prasannakumara B C and Punith Gowda R J 2022 *Waves Random Complex Media* 1
[41] Yusuf T A, Mabood F, Khan W A and Gbadeyan J A 2020 *Alex. Eng. J.* **59** 5247
[42] Waqas H, Imran M and Bhatti M M 2021 *Eur. Phys. J. Spec. Top.* **230** 1317
[43] Hayat T, Aziz A, Muhammad T and Alsaedi A 2019 *J. Braz. Soc. Mech. Sci. Eng.* **41** 1
[44] Tijani Y O, Akolade M T and Mohd Kasim A R 2023 *J. Comput. Theor. Transp.* **52** 343
[45] Khan W A and Pop I 2010 *Int. J. Heat Mass Transfer* **53** 2477
[46] Reddy Gorla R S and Sidawi I 1994 *Appl. Sci. Res.* **52** 247
[47] Al-Kouz W and Owhaib W 2022 *Sci. Rep.* **12** 4256
[48] Dawar A, Islam, S, Shah Z and Mahmuod S R 2023 *J. Mol. Liq.* **382** 122018